Chemical Geology 545 (2020) 119648

Contents lists available at ScienceDirect

Chemical Geology

journal homepage: www.elsevier.com/locate/chemgeo

High-precision molybdenum isotope analysis of low-Mo igneous rock samples by MC–ICP–MS

Jing-Jing Fan[a,b], Jie Li[a,*], Qiang Wang[a,b,c], Le Zhang[a], Jing Zhang[a,b], Xiang-Lan Zeng[a,b], Lin Ma[a], Zi-Long Wang[a,b]

[a] State Key Laboratory of Isotope Geochemistry, Guangzhou Institute of Geochemistry, Chinese Academy of Sciences, Guangzhou 510640, China
[b] College of Earth and Planetary Sciences, University of Chinese Academy of Sciences, Beijing 100049, China
[c] CAS Center for Excellence in Tibetan Plateau Earth Science, Beijing 100101, China

ARTICLE INFO

Editor: Balz Kamber

Keywords:
Molybdenum isotopes
Low-Mo rock
Chromatographic exchange
Leucogranites
MC–ICP–MS

ABSTRACT

Recent advances in analytical techniques have achieved high-precision ($2\sigma \leq 0.06‰$) determinations of Mo isotopic ratios in silicate rocks but few such data are as yet available, especially for low-Mo (< 50 ppb) rocks such as leucogranites. Here we present two low-blank, double-spike, high-yield, ion-exchange chromatographic methods (single- and two-column) for precise determination of Mo isotopic ratios in low-Mo rock samples (10–500 ppb) using multicollector–inductively coupled plasma–mass spectrometry (MC–ICP–MS). The two-column technique involved AG 1-X8 anion-exchange (100–200 mesh) and BPHA chelatin resins, with the latter also used in the single-column procedure. Two USGS reference materials (basalt BIR-1a and diabase W-2a) were analyzed for quality-control purposes. Their $\delta^{98/95}$Mo values determined using the two methods are consistent within uncertainties, and with those determined by previously published methods. We provide the first Mo isotopic data for the reference materials of dunite DTS-2b (USGS), GPt-3 (NRCG) and peridotite WPR-1 (CCRMP). $\delta^{98/95}$Mo values for DTS-2b and WPR-1 by using two-column procedure are in good agreement with those obtained by single-column separation. Repeated analyses of these standards indicate a long-term external reproducibility of better than ± 0.05‰. However, the $\delta^{98/95}$Mo values of GPt-3 show poor reproducibility due to either the sample heterogeneity or existing undigested minerals (e.g., spinel). The methods were applied to leucogranites with low Mo contents of 10–74 ppb from the Himalaya orogen and southern Lhasa terrane of Tibet. The isotopic analyses yielded $\delta^{98/95}$Mo values of −0.2‰ to 0.34‰ and −0.41‰ to −0.68‰ (against NIST SRM 3134), respectively, within the range of values for igneous crust. Their contrasting Mo isotopic compositions may indicate compositional diversity in their sources or differences in magma evolution.

1. Introduction

Stable Mo isotopes have been widely applied to marine sediments for paleo-redox reconstruction (Siebert et al., 2003; Anbar, 2004; Pearce et al., 2008; Gordon et al., 2009; Planavsky et al., 2014), which is based on the significant Mo isotopic fractionation (~3‰) between oxic marine sediments and seawater (Barling et al., 2001; McManus et al., 2002; Siebert et al., 2003; Anbar, 2004; Tossell, 2005; Dickson, 2017) and high Mo contents (up to 200 ppm) of marine sediments (Scott and Lyons, 2012) in low-temperature settings. Recently, more and more studies on igneous systems using Mo isotopes have emerged, and the fractionation can be up to 2‰ (Greber et al., 2015; Yang et al., 2015, 2017; König et al., 2016; Chen et al., 2019; Li et al., 2019; Zhang et al., 2019). Meteorites, arc volcanic rocks, mid-ocean-ridge basalts (MORB), and ocean-island basalts (OIB) have relatively high Mo contents averaging 3.6, 0.9, 0.6, and 4.3 ppm, respectively (Jenner and O'Neill, 2012; Voegelin et al., 2012; Burkhardt et al., 2014; Freymuth et al., 2015, 2016; Bezard et al., 2016; König et al., 2016; Gaschnig et al., 2017; Liang et al., 2017). A growing number of studies of these rocks define discernable high-temperature Mo reservoirs and contribute to the understanding of the formation and chemical differentiation of the Earth. The behavior of Mo isotopes in terrestrial samples has been used to trace magma formation and evolution (Voegelin et al., 2014; Wille et al., 2018; Casalini et al., 2019), crustal material recycling (Freymuth et al., 2015, 2016; König et al., 2016; Li et al., 2019), and mantle source heterogeneity (Bezard et al., 2016). However, there are few reports concerning Mo isotopes in rocks with low or ultra-low Mo contents (10–100 ppb), which include mantle-derived rocks

* Corresponding author.
E-mail address: jieli@gig.ac.cn (J. Li).

https://doi.org/10.1016/j.chemgeo.2020.119648
Received 22 December 2019; Received in revised form 15 April 2020; Accepted 27 April 2020
Available online 29 April 2020
0009-2541/

(39–47 ppb; Palme and O'Neill, 2004; Greber et al., 2015) and granites (< 100 ppb; Luais and Hawkesworth, 1994; Whalen et al., 2002, 2003), for which Mo isotopic variations constrain the composition and evolution of the mantle and crust, respectively. Ultra-low Mo contents also occur in non-euxinic sediments such as carbonates and phosphorites, which may be used to trace paleo-oceanic redox conditions (Voegelin et al., 2009; Wen et al., 2015). However, the low Mo contents of these rocks require large sample amounts (1–5 g) for isotopic analysis, which poses challenges for Mo extraction from such large volumes of sample matrices and overcoming isobaric interferences. Efficient and convenient methods for Mo purification and analysis are therefore required for low-Mo samples.

Numerous protocols have been developed for the separation and purification of Mo from Mo-rich geological samples involving different resins, acids, or chromatographic column specifications. These protocols can quantitatively separate Mo from matrix elements such as Fe, Co, Ni, Se, Pt, Cu, Zn, Ge, and Ru which might be involved to form polyatomic interferences on the four Mo isotopic masses (^{95}Mo, ^{97}Mo, ^{98}Mo, ^{100}Mo) that are used for the double spike deconvolution (e.g., $^{59}Co^{36}Ar^{+}$ on ^{95}Mo, $^{40}Ar^{57}Fe$ on ^{97}Mo, $^{58}Ni^{40}Ar^{+}$ on ^{98}Mo, $^{70}Ge^{14}N^{16}O^{+}$ on ^{100}Mo; Table 1) (Qi and Masuda, 1994; Anbar et al., 2001; Dauphas et al., 2001; Siebert et al., 2001; Malinovsky et al., 2005; Pietruszka et al., 2006; Nakagawa et al., 2008; Pietruszka and Reznik, 2008; Pearce et al., 2009; Li et al., 2014; Liu et al., 2016; Feng et al., 2019). Barling et al. (2001) and Siebert et al. (2001) adopted a two-column ion-exchange procedure for Mo purification involving an anion-exchange column (AG 1-X8) for separation of Zr and Mn from Mo, followed by a cation-exchange column (AG 50 W-X8) to remove Fe. Pietruszka et al. (2006) improved this method and achieved a high Mo recovery of 98%–100% with a low Mo blank of 0.8 ng. Single-column separation methods are generally convenient and less time-consuming. Malinovsky et al. (2005) and Pearce et al. (2009) developed single-column Mo separation techniques using the chelating resin Chelex 100 and anion-exchange resin AG 1-X8, respectively. A more efficient technique with lower elution volumes was reported by Li et al. (2014) based on N-benzoyl-N-phenylhydroxylamine (BPHA) supported on a microporous acrylic ester polymeric resin (Amberlite CG-71), also with high recovery (~100%) and low procedural blank (~0.18 ng). However, there is a lack of methods developed specifically for low-Mo rock samples, and high-precision $\delta^{98/95}$Mo data for low-Mo rock standards are rare. Willbold et al. (2015) reported a new low-volume, single-pass anion-exchange separation technique that can cope with large sample amounts while maintaining low blank levels and short processing times. However, just one low-Mo (~30 ppb) United States Geological Survey (USGS) reference material of BIR-1 that is a typical mid-ocean-ridge basalt was analyzed. It is not clear whether this method is suitable for other types of low-Mo reference materials such as USGS dunite DTS-2b and National Research Center of Geoanalysis, China (NRCG) dunite Gpt-3. A two-step ion-exchange chromatography technique has recently been proposed by Liu et al. (2016) to purify Mo from low-Mo rock samples. Nevertheless, all the low-Mo samples have been limited to sedimentary rocks such as dolomite, phosphorite, and siliceous sand with Mo contents > 60 ppb. The higher matrix/Mo ratios of low-Mo samples such as peridotites and leucogranites mean that purification is more difficult than for high-Mo samples. Effort towards facilitating Mo isotopic ratio determinations in geological samples with low Mo contents (< 50 ppb) is clearly needed.

Here we report two efficient Mo separation methods for low-Mo rock samples: a two-column ion-exchange technique involving anion-exchange (AG 1-X8) and BPHA columns; and an improved single-column purification procedure utilizing BPHA, modified from that of Li et al. (2014). We compared the precision, accuracy, and efficiency of these two new techniques by analyzing a range of low-Mo silicate reference and natural materials. One commonly used reference material, USGS W-2a with a relatively high Mo content (~0.4 ppm), was also analyzed for quality-control purposes. Here we describe efficient, fast, and low-blank extraction protocols for quantitatively separating Mo from low-Mo igneous samples, allowing determination of < 1‰ Mo isotopic fractionation in high-temperature geological processes. We also report high-precision Mo isotopic data for leucogranites from Tibet as a step towards understanding the Mo isotope reservoir of continental crust.

2. Samples and analytical techniques

2.1. Samples

Leucogranites were collected for Mo isotopic analysis, including 9 from the Tsona and Saga areas in the eastern and western Himalaya and 4 from the Zhengga area in the southern Lhasa terrane, with these areas being separated by the Yarlung Tsangpo suture zone. The rock types are two-mica granite (TMG) and garnet-bearing leucogranite (GBG). All samples were fresh with little or no discoloration or evidence of altered minerals or alteration phases. The samples were crushed into small

Table 1
Major potential interferences on Mo isotopes.

Mass	Oxide ions	Argide ions	Nitrogen monoxide	Chloride ions	Isobars	Doubly charged ions
^{92}Mo	$^{76}Se^{16}O+$ $^{76}Ge^{16}O^{+}$ $^{75}As^{17}O^{+}$	$^{54}Fe^{38}Ar^{+}$ $^{54}Cr^{38}Ar^{+}$	$^{62}Ni^{14}N^{16}O^{+}$ $^{59}Co^{15}N^{18}O^{+}$	$^{57}Fe^{35}Cl^{+}$ $^{55}Mn^{37}Cl^{+}$	$^{92}Zr+$	$^{184}W^{2+}$ $^{184}Os^{2+}$
^{94}Mo	$^{78}Se^{16}O^{+}$	$^{56}Fe^{38}Ar+$ $^{54}Fe^{40}Ar^{+}$ $^{58}Ar^{36}Ar+$ $^{54}Cr^{40}Ar^{+}$	$^{63}Cu^{15}N^{16}O^{+}$ $^{64}Zn^{14}N^{16}O^{+}$ $^{62}Ni^{14}N^{18}O^{+}$	$^{57}Fe^{37}Cl^{+}$ $^{59}Co^{35}Cl+$		$^{188}Os^{2+}$
^{95}Mo	$^{78}Se^{16}OH^{+}$	$^{55}Mn^{40}Ar+$ $^{57}Fe^{38}Ar^{+}$ $^{59}Co^{36}Ar+$	$^{65}Cu^{14}N^{16}O^{+}$ $^{64}Zn^{15}N^{16}O^{+}$	$^{58}Ni^{37}Cl+$ $^{58}Fe^{37}Cl^{+}$		$^{190}Os^{2+}$
^{96}Mo	$^{80}Se^{16}O+$	$^{56}Fe^{40}Ar+$ $^{58}Ni^{38}Ar^{+}$	$^{65}Cu^{15}N^{16}O^{+}$ $^{66}Zn^{14}N^{16}O^{+}$ $^{64}Ni^{14}N^{18}O^{+}$	$^{61}Ni^{35}Cl^{+}$ $^{59}Co^{37}Cl^{+}$	^{96}Zr ^{96}Ru	$^{192}Os^{2+}$ $^{192}Pt^{2+}$
^{97}Mo	$^{80}Se^{16}OH^{+}$	$^{57}Fe^{40}Ar^{+}$ $^{59}Co^{38}Ar^{+}$ $^{61}Ni^{36}Ar+$	$^{65}Cu^{14}N^{18}O^{+}$	$^{60}Ni^{37}Cl^{+}$		$^{194}Pt^{2+}$
^{98}Mo	$^{82}Se^{16}O^{+}$	$^{58}Ni^{40}Ar^{+}$ $^{58}Fe^{40}Ar^{+}$	$^{68}Zn^{14}N^{16}O^{+}$	$^{63}Cu^{35}Cl^{+}$ $^{61}Ni^{37}Cl^{+}$	$^{98}Ru^{+}$	$^{196}Pt^{2+}$
^{100}Mo	$^{84}Sr^{16}O^{+}$	$^{60}Ni^{40}Ar^{+}$ $^{64}Zn^{36}Ar^{+}$	$^{68}Zn^{14}N^{18}O^{+}$ $^{69}Ga^{15}N^{16}O^{+}$ $^{70}Ge^{14}N^{16}O^{+}$	$^{63}Cu^{37}Cl^{+}$	$^{100}Ru^{+}$	$^{200}Hg^{2+}$

Table 2
Mo chemical separation procedure 1 on strongly anionic exchange resin (AG 1-X8, 100–200 mesh, 1 mL) combined with BPHA resin (0.2–0.3 mL).

Process	Reagent	Volume/mL
Column #1: 1 mL AG 1-X8 (100–200 mesh)		
Clean	2 M HNO_3	4–6
Condition	0.5 M HCl – 0.5 M HF	4–6
Load sample	Sample solution	6–12
Wash	0.5 M HCl – 0.5 M HF	8–10
Collect Mo	2 M HNO_3	6
Column #2: 0.2–0.3 mL BPHA resin		
Clean	6 M HF	2
Condition	1 M HNO_3 – 0.1 M HF	2
Load sample	Sample solution	12
Wash	1 M HNO_3–0.1 M HF	8
Collect Mo	6 M HF	8

chips (~2 cm), and the freshest fragments were hand-picked, cleaned with 1% HCl, washed ultrasonically in deionized water, air dried, and powdered to 200 mesh in an agate mill for chemical analyses.

2.2. Reagents and materials

High-purity deionized water (resistivity 18.2 MΩ cm) from a Milli-Q water-purification system (Millipore, Bedford, MA, USA) was used throughout this study. All acids were ultra-pure grade, including concentrated hydrofluoric acid (24 M) and hydrochloric acid (12 M) purified by DST-1000 sub-boiling stills (Savillex Corporation, USA), and concentrated nitric acid (16 M). The resins used were high-purity AG Muromac® 1-X8 (Cl^-) anion-exchange resin (100–200 mesh), BPHA (Analytical grade; Aladdin Reagents, China), and Amberchrom CG-71 (50–100 μm; Supelco, USA). A natural sample solution (USGS reference material of BCR-2 with high Mo content of 248 ppm) and a synthetic multi-element solution with a concentration of 1 ppm prepared from AccuStandard fluoride-soluble elements (MISA 05-1 containing Ti, Ge, Zr, Hf, Nb, Ta, Mo, W, Sn and Sb) were used in optimizing column separation parameters. US National Institute of Standards and Technology (NIST) SRM 3134 (Lot No. 891307) was used as a Mo isotopic reference material for assessing long-term repeatability of MC–ICP–MS analyses and in investigating Mo isotopic fractionation during column chemistry. A ^{97}Mo–^{100}Mo double-spike solution was prepared as a mixture of individual concentrated solutions of isotopically enriched ^{97}Mo (Batch 159791) and ^{100}Mo (Batch 159992) purchased from Oak Ridge National Laboratory, USA, and calibrated earlier (Li et al., 2014).

2.3. Purification of BPHA resin

BPHA supported on microporous acrylic ester polymeric resin (Amberlite CG-71) is stable in highly acidic solutions and can efficiently preconcentrate Zr, Hf, Nb, Ta, Ti, Mo, and W from rock sample solutions (Caletka and Krivan, 1989; Goguel, 1992; Yang and Pin, 2002; Shinotsuka and Suzuki, 2007; Li et al., 2010, 2014). Unpurified BPHA resin was used by Li et al. (2014) to isolate Mo from geological samples with relatively high Mo contents. However, for low-Mo samples, it may be a significant contributor to blanks, and rigorous purification of both BPHA and CG-71 is required.

BPHA was purified by recrystallization from aqueous/ethanol solution. BPHA (3 g) was dissolved in ethanol and mixed with 400 mL Milli-Q water at 80 °C, and it began to crystallize as the mixture cooled to room temperature. The aqueous/ethanol solution was then removed from the crystals by filtration, and the recrystallized BPHA was redissolved in ethanol for the next step. CG-71 was washed with a mixture of ethanol +6 M HCl + water (2:1:1). After at least three times of vibration, the mixture was allowed to stand overnight, then, pour out the supernatant. The CG-71 was then rinsed with deionized water until the resin was free from acid. The purified CG-71 resin was impregnated with a purified BPHA-ethanol solution by shaking at room temperature (25 °C) for 30 min to ensure complete saturation. It was then stored in a refrigerator prior to use (Li et al., 2014).

2.4. Sample preparation and digestion

All sample preparation and digestion work was undertaken in a Class 1000 clean laboratory equipped with Class 100 laminar-flow exhaust hoods. Sample powder (0.3–3.0 g) and an appropriate amount of ^{97}Mo–^{100}Mo double-spike solution were weighed accurately in 15–50 mL PFA beakers. The double-spike solution was added to account for Mo isotopic fractionation during column separation and to correct the instrumental mass bias during mass spectrometric analyses (Siebert et al., 2001; Zhang et al., 2018). Samples were dissolved in HF + HNO_3 volumes appropriate for the sample size: for ~3 g samples, ~4 mL 8 M HNO_3 + 8 mL 24 M HF were used. The closed beakers were heated on a hotplate at 150 °C for at least 3 d. To aid sample digestion, the mixture was agitated occasionally for ~5 min in an ultrasonic bath. After digestion, the solutions were evaporated to incipient dryness at 120 °C and the residue dissolved in 6 M HCl to remove the fluorides. After re-evaporation, the residue was dissolved in 6–12 mL 0.5 M HCl + 0.5 M HF or 0.2 M HF + 1 M HCl/HNO_3 (why the choice was made between HCl and HNO_3 is further discussed below). Subsequently, the residue was separated from the solution by centrifugation, and the solution was transferred into 15 mL centrifugal tubes for double and single-column separation.

2.5. Chemical purification

Double- (Table 2) and single-column (Table 3) Mo purification techniques were used for comparative purposes in processing large samples (2–3 g). A Bio-Rad Poly-Prep® column (Bio-Rad Laboratories, Berkeley, CA, USA) with ca. 0.8 cm inner diameter and ca. 4 cm resin bed height was used to reduce processing time in these procedures.

2.5.1. Double-column separation

The strongly anionic exchange resin AG 1-X8 (100–200 mesh, 1 mL) was used first to remove matrix elements such as Fe, Cu, Ni, Mn, Sr, and Ca (Pearce et al., 2009). The BPHA resin (0.2–0.3 mL) was then used to separate Mo from residual fluoride-soluble elements such as Ti, Zr Hf, Nb, Sn, Sb, and W (Li et al., 2014). The high-purity anion-exchange resin AG 1-X8 was cleaned using 4–6 mL 2 M HNO_3 and Milli-Q water before conditioning with a 0.5 M HCl + 0.5 M HF mixture (acidity matching that of the sample solution). The sample solution (8–12 mL) corresponding to 0.3–3 g of digested sample without any residue was loaded onto the column, and the resin was washed with 8–10 mL 0.5 M HCl + 0.5 M HF. Then, the adsorbed Mo and other elements such as Ti and Zr were eluted in 6 mL 2 M HNO_3. This procedure was checked routinely by analysis of a well-characterized rock standard of USGS BCR-2 (Fig. 1a).

Matrix elution from the BPHA column has been achieved by using a mixture of HCl and HF (Li et al., 2014). However, it was unknown whether BPHA resin can successfully elute matrix elements with dilute mixture of HNO_3 and HF. We chose the mixture of dilute HNO_3 (1 or

Table 3
Mo chemical separation procedure 2 on BPHA resin (0.3–0.5 mL).

Process	Reagent	Volume/mL
0.3–0.5 mL BPHA resin		
Clean	6 M HF	2
Condition	1 M HNO_3 (HCl) – 0.2 M HF	2
Load sample	Sample solution	6–12
Wash	1 M HNO_3 (HCl) – 0.2 M HF	8–12
Collect Mo	6 M HF	8

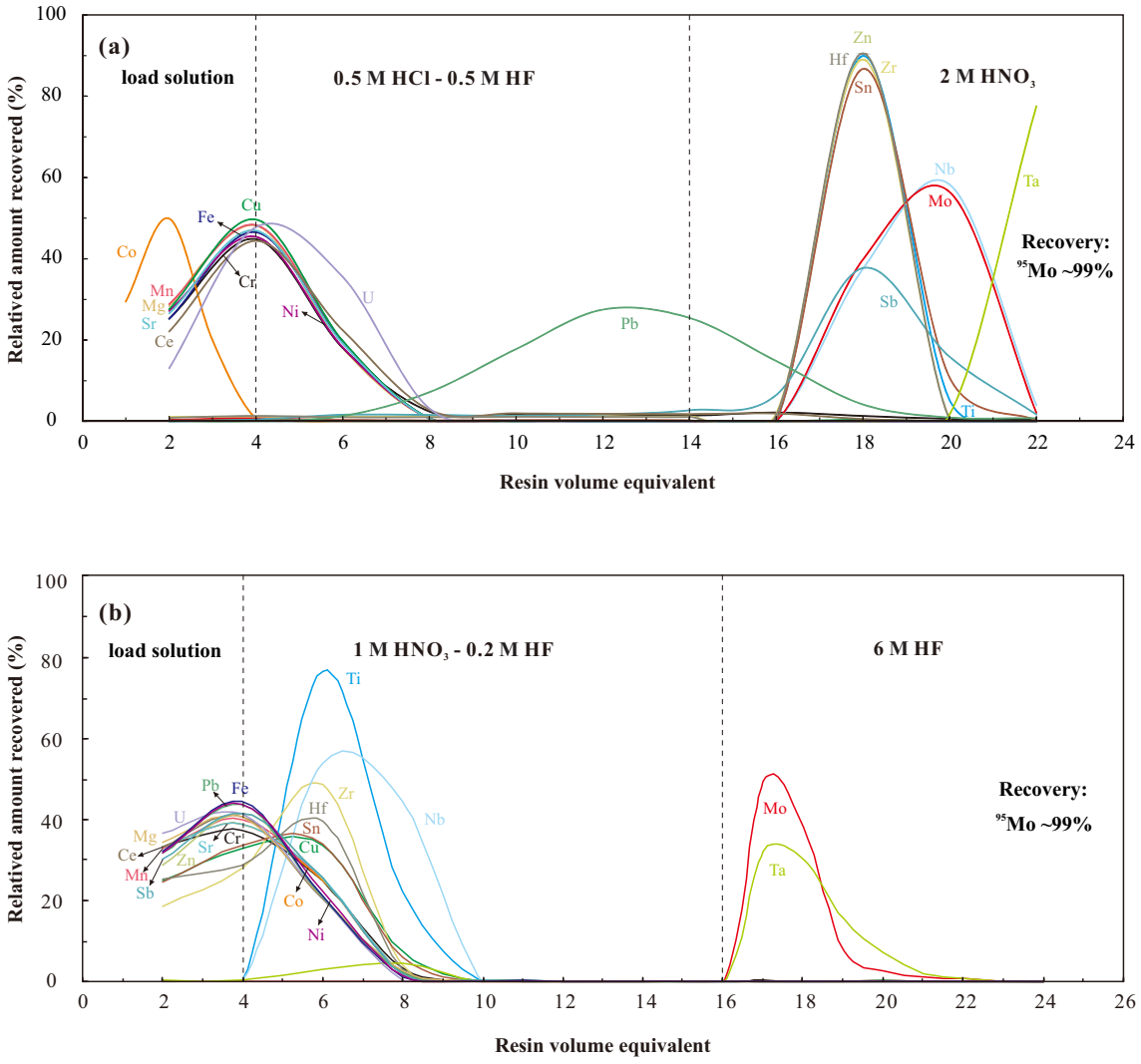

Fig. 1. Elution curves for selected major and trace elements in analyses of basalt standard of BCR-2 with an AG 1-X8 anion-exchange column (a) and BPHA resin column (b).

2 M) and HF (0.2 M) to separate Mo and test the purification efficiency of different acids. A simple synthetic multi-element solution was used for testing the elution behavior of Mo and some matrix elements on the BPHA resin. Results indicate that excellent separation is achieved with 1 M HNO_3 + 0.2 M HF (Fig. 2a) as eluent, while Mo loss occurs during eluted by 2 M HNO_3 + 0.2 M HF (Fig. 2b). The elution curves for selected major and trace elements using the same natural rock standard solution (BCR-2) and employing the eluent of HNO_3 and HF also show that Mo can be separated completely (Fig. 1b). Based on this, the Mo fraction in 2 M HNO_3 from the preceding anion-exchange column can be diluted with an equal volume of 0.2 M HF and loaded directly onto the BPHA column. This eliminated a drying/redissolution step and reduced the likelihood of cross-contamination, although the relatively large volume of acids involved made the procedure more time consuming.

2.5.2. Single-column separation

BPHA resin can efficiently remove most cations, including Fe, Mn, Cr, Ni, Cu, Sr, Rb, La, and Th (Li et al., 2014). We therefore considered that the isolation of Mo from low-Mo samples could be achieved solely by BPHA resin with increased concentration and volume of the eluent HF, and more resin (Table 3). For samples with low Mo contents (< 50 ppb) or significantly high matrix-element (e.g., Fe, Mn, Ti) contents, the HF concentration was increased to 0.3 M.

The collected Mo was evaporated to dryness on a hot plate at 120 °C. Compared with the double-column separation technique, the single-column procedure produced a larger mass of residue due to the increase in organic matter associated with the larger volume of BPHA. The organic matter was decomposed by treatment with three drops of concentrated HNO_3 and H_2O_2. Following this, 0.5 mL of 3% (v/v) HNO_3 was added to the Mo residue, after which the solution was ready for Mo isotopic ratio measurement by MC–ICP–MS (Li et al., 2014; Zhao et al., 2016).

2.6. Mass spectrometry

Mo isotopic analyses were performed at the State Key Laboratory of Isotope Geochemistry, Guangzhou Institute of Geochemistry, Chinese Academy of Sciences (SKLaBIG, GIG-CAS), Guangzhou, China, using a Thermo Fisher Scientific Neptune plus MC–ICP–MS system. The instrument incorporates nine Faraday cups and eight ion counters, which were linked to amplifiers with 10^{11} Ω resistors. It was equipped with a newly designed large dry-interface pump (100 m^3 h^{-1}) and an X skimmer cone, which significantly improved instrument sensitivity. The operational settings of the mass spectrometric source are given in Table 4. Commonly, low-content samples are commonly performed under dry-plasma condition through an Aridus II desolvator to remove water from the sample solutions, which can indeed improve the

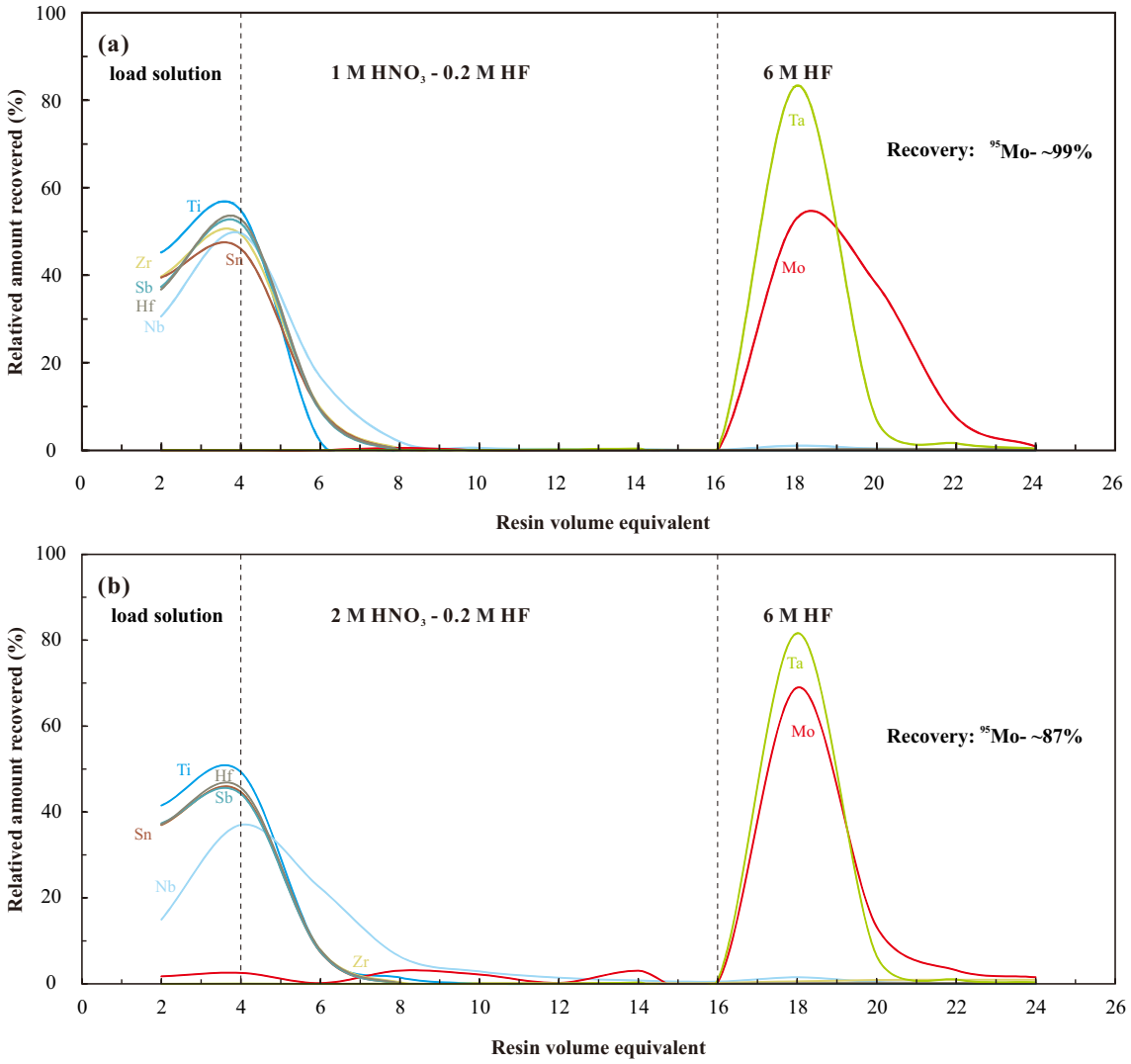

Fig. 2. Elution curves for selected major and trace elements in analyses of a synthetic multi-element solution with BPHA resin column with different concentrations of HNO_3 eluent: 1 M HNO_3 + 0.2 M HF (a) and 2 M + 0.2 M HF (b).

Table 4
Typical instrumental setup used during MC-ICP-MS analysis in this study.

Instrument	Neptune plus
RF power	1180 W (optimized daily)
Auxiliary gas (Ar) flow rate	0.98 L min^{-1} (optimized daily)
Sample gas (Ar) flow rate	0.975 L min^{-1} (optimized daily)
Cooling gas (Ar) flow rate	16.00 L min^{-1}
Measurement mode	Static
Interface cones	H sample cone +X skimmer cone (nickel)
Acceleration voltage	10 kV
Detection system	L4 (^{91}Zr), L2 (^{94}Mo), L1 (^{95}Mo), C (^{96}Mo), H1 (^{97}Mo), H2 (^{98}Mo), H3 (^{99}Ru), H4 (^{100}Mo)
Amplifier	10^{11} Ω
Integration time	4.19 s
Mass resolution	400 (low)
Sensitivity	1.2–1.5 V for ^{98}Mo at 100–150 ppb Mo
Blocks and cycles	one blocks x 40–50 cycle
Nebulizer	MicoFlow PFA-50; speed: 50 μL min^{-1}
Spray chamber	Dual cyclonic-Scott (quartz)

sensitivity of MC-ICP-MS (e.g., 5–7 V for ^{98}Mo at 50 ppb Mo, Feng et al., 2019). However, this sample-introduction system in our lab would produce a notable memory effect, which makes the residual Mo signal hardly to be washed down, and further results in the instability of the instrument. Thus, we choose the wet-plasma method. Samples were usually diluted to about 150–200 ppb concentration for Mo isotope analysis and the typical signal with this set up on ^{98}Mo was ~1.5 V. For samples with Mo with concentrations of ~10 ng, digestion of ~3 g of sample material can obtain of ~60 ppb Mo solution with ^{98}Mo signal of ~0.5 V, which is within the detection range. Sample and reference solutions were introduced into the MS in 2% (v/v) HNO_3 using a self-aspiration PFA nebulizer (50 μL min^{-1}) and a dual cyclonic spray chamber. High Mo sensitivities and low Mo uptake rates were achieved for isotopic analyses of low-Mo solutions. Data were acquired in one block of 40–50 cycles with an integration time of ~4.2 s per cycle. After each analysis, the inlet was washed for 3 min in 2% v/v HNO_3, 2% HNO_3 + 0.01% HF, and 2% v/v HNO_3 with the residual ^{98}Mo signal typically being < 0.5 mV.

Prior to starting an analytical session, the reference solution (a mixture of NIST SRM 3134 and ^{97}Mo–^{100}Mo double-spike solutions) was analyzed typically five times to check MC–ICP–MS performance, and thereafter the reference solution was analyzed after each batch of three samples. The double-spike method (Siebert et al., 2001) is the most precise mass-bias correction procedure, and was adopted to account for isotopic fractionation during chemical separation and instrumental analysis. Double-spike isotopic calculations involved an in-

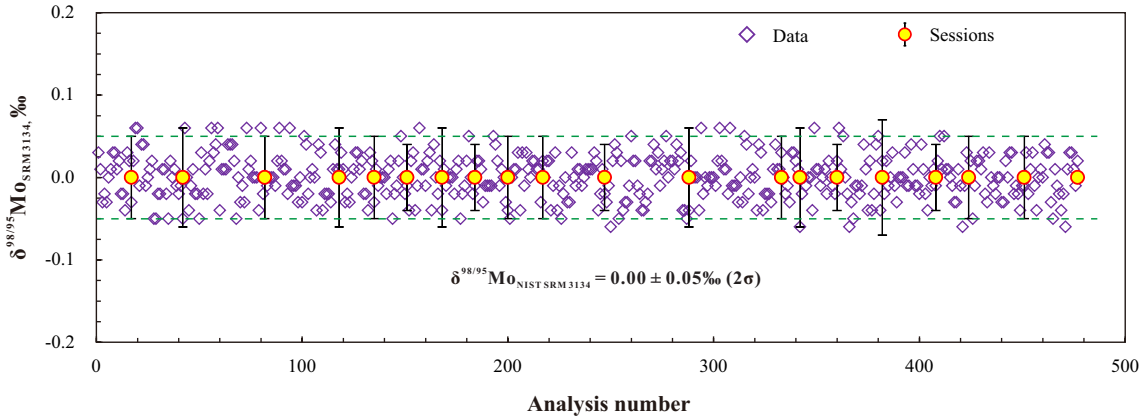

Fig. 3. Stability of Mo isotopic compositions ($\delta^{98/95}$Mo values) of NIST SRM 3134 over a period of 2 years. The green dashed lines indicate ± 2σ from the mean value. (For interpretation of the references to colour in this figure legend, the reader is referred to the web version of this article.)

house Microsoft Virtual Basic program based on a mathematical algorithm described by Zhang et al. (2015). All standard/double-spike mixtures had $^{98}Mo/^{100}Mo$ ratios in the range of 0.3–0.6, verified as having no significant effect on $\delta^{98/95}$Mo results (Zhang et al., 2018). Sample Mo isotopic ratios were normalized to those of NIST SRM 3134 and expressed as follows:

$$\delta^{98/95}\text{Mo}\ (‰) = [(^{98}Mo/^{95}Mo)_{sample} - (^{98}Mo/^{95}Mo)_{SRM\,3134}] / (^{98}Mo/^{95}Mo)_{SRM\,3134} \times 1000 \quad (1)$$

The precision of Mo isotope ratio analyses was assessed by the results obtained in the bracketing standards of NIST SRM 3134, assuming that the standard deviation (σ) of the sample measurements equals to the standard deviation of the bracketing standard measurements. The standard deviation of $\delta^{98/95}$Mo value was 0.05‰ (2σ) (Fig. 3) based on the results of NIST SRM 3134 with ~500 analyses over 20 measurement sessions during a period of 2 years, indicating that the long-term repeatability of our instrument was < 0.05‰ (2σ).

3. Results and discussion

The accurate determination of Mo isotopic compositions requires high Mo recoveries and avoidance of matrix-element interference effects during chemical procedures, as well as reduction of acidity, concentration, and memory effects during isotopic analysis. It has been reported that Mo isotopic analyses with different instruments can produce variable degrees of sensitivity to HNO_3 concentrations in the aspirated solution (Malinovsky et al., 2005; Li et al., 2010), although the acidity effect with 1%–2% (v/v) HNO_3, as used here, is negligible with the Neptune plus MC–ICP–MS (Liu et al., 2016). The concentration effect can also be reduced if the concentration ratio between standard and sample is < 50% (Rudge et al., 2009; Liu et al., 2016). The memory effect means that a Mo isotopic analysis is influenced by the previously analyzed sample (Helz et al., 1996), although with the reduction of the residual ^{98}Mo signal to < 1 mV after 3 min of washing, this effect is negligible.

In the following sections we assess the effectiveness of the two chemical treatment techniques on Mo isotopic analyses of reference and geologic samples.

3.1. Matrix separation

Matrix elements can cause significant spectral and non-spectral interferences in Mo isotopic analyses, especially for low-Mo samples. The most important isobaric interferences include Fe, Ti, Mn, Cr, Ni, Cu, Co, Zn, and Sr (Table 1). With the strongly anionic exchange resin, a mixture of low-molarity HCl and HF (0.5 M) can elute Fe, Mn, Cu, Co, Cr, Ni, U, Mg, Sr, and Ce, and an additional BPHA column step is then required to further separate Mo from other elements such as Zr, Hf, Ti, Nb, Sn, Sb, Zn, Pb, and W (Fig. 1a, b; Li et al., 2014). After the two column steps, Mo is entirely isolated from most matrix elements, with most X/Mo ratios (where X represents an isobarically interfering element) being < 1%, except for Ta (Fig. 4a, b), although interference by Ta has proved insignificant with BPHA resin (Li et al., 2014) and the use of an anion-exchange resin reduces the amount of Ta collected (Fig. 1a). The probability of the other spectral interferences originating from doubly charged ions (e.g., Os, Pt and Hg) and from refractory oxides (e.g., Se and Ge) is considered very low because most of these elements are present at trace level in geological samples and are readily separated from Mo during the purification procedure (Malinovsky et al., 2005). The single-column method with BPHA resin can also effectively isolate Mo from interfering matrix elements (Fig. 1b; Li et al., 2014), although for samples with low Mo/matrix-element ratios the concentrations and volumes of eluents must be adjusted to avoid Mo loss while eluting matrix elements.

Isotopic fractionation of Mo is known to occur during its isolation due to incomplete Mo recovery (e.g., Anbar et al., 2001; Siebert et al., 2001; Pietruszka and Reznik, 2008). We studied isotopic fractionation during chemical separation with the anion-exchange and BPHA resins. The recovery of Mo was determined by comparing the measured ^{95}Mo signal in the unpurified sample solution with that of all elution aliquots, taking into account the dilution factors and sample mass. Mo recoveries measured from the unspiked reference sample solutions both with anion-exchange resin and BPHA resin were ~99%. With such high recovery rates and the double-spike method of mass-bias correction, Mo isotopic fractionation during chemical separation can be ignored. The methods presented here also significantly reduce the time required for Mo separation, with the two-column method being completed in > 8 h. Previously reported two-column procedures required > 24 h due to the need for drying of the Mo fraction after the first column separation (Pietruszka et al., 2006; Wasylenki et al., 2008; Zhang et al., 2009; Burkhardt et al., 2014; Voegelin et al., 2014; Greber et al., 2015; Liu et al., 2016; Gaschnig et al., 2017). The whole purification procedure with a single BPHA column can be completed in > 2 h, and this is possibly the most rapid Mo isolation method reported to date.

3.2. Total procedural blanks

Resins and acids are the predominant contributors to high Mo blanks, which may have significant effects on Mo isotopic analyses, especially for low-Mo geological samples. Here we assessed procedural blanks by processing the usual quantities of acids through the whole column procedure, from sample digestion to Mo collection, as for

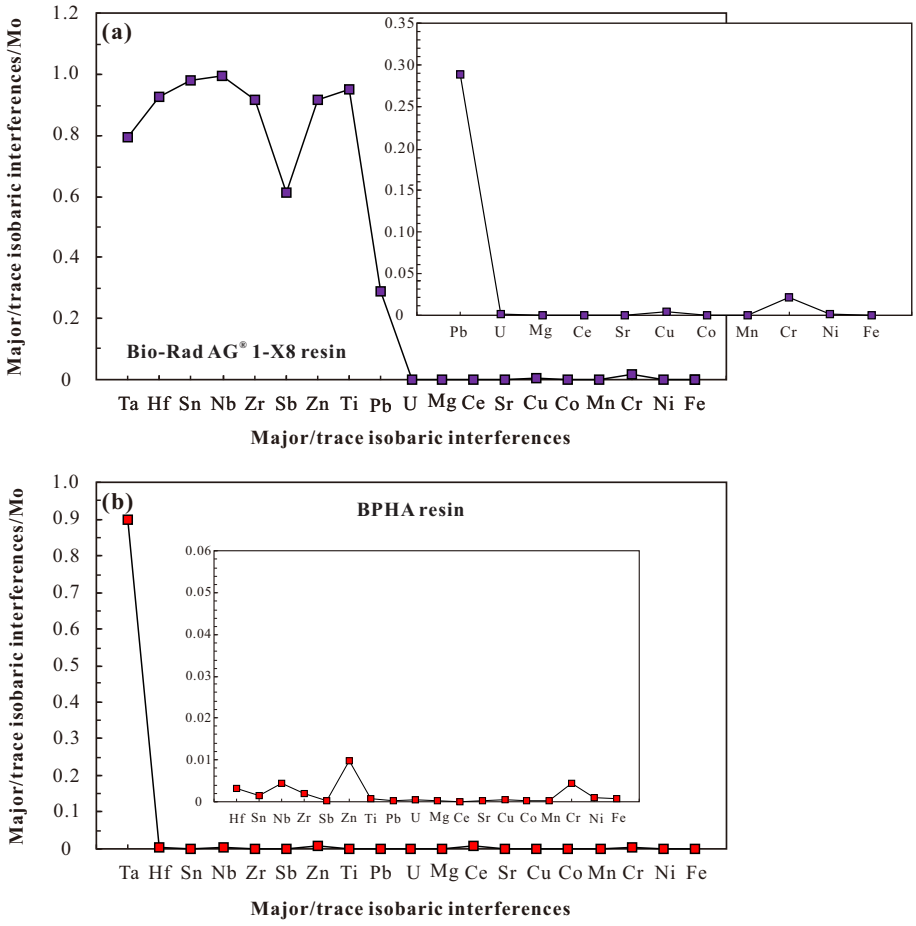

Fig. 4. Residual matrix and isobaric-interference elements eluted from rock standard sample of BCR-2 by using AG 1-X8 anion (a) and BPHA (b) resins.

regular samples.

For the two-column method of Mo purification, with 1 mL AG 1-X8, 0.3 mL BPHA, and the usual reagents, Mo blanks were in the range of 7–14 pg, while the single-column method with purified BPHA yielded a blank of ~3 pg Mo, lower than that obtained with unpurified BPHA resin (~200 pg). Total procedural Mo blanks for the double- and single-column methods were in the ranges 90–190 pg (mean 123 ± 54 pg; 2σ; n = 11) and 30–120 pg (mean 81 ± 58 pg; 2σ; n = 13), respectively. Given that the total procedural Mo blanks (30–190 pg either for the single or the double column methods) relative to the amount of sample Mo processed (30–120 ng) are < 1%, this low blank levels thus had no significant effect on the measured Mo isotopic compositions of the low-Mo samples.

3.3. Precision and accuracy

Precision and accuracy was determined through replicated analyses of standards involving separate digestions of the same rock powder followed by purification by different separation techniques (double- or single-column) or different eluents (HNO_3 or HCl), and repeated column purification of the bulk raw solutions from the same rock powder. Five reference materials were analyzed: USGS basalt BIR-1a, dunite DTS-2b, diabase W-2a, CCRMP (Canadian Certified Reference Materials Project) peridotite WPR-1, and NRCG dunite GPt-3. Analytical results are presented in Table 5, together with previously reported data.

Our Mo content analyses exhibit a good reproducibility with 2σ ranging from 0.001 to 0.04 for ppm, regardless of sample composition and digestion or purification method, except for peridotite GPt-3. Results of analyses by three methods are considered here, involving (1) single-column (HCl eluent), (2) single-column (HNO_3 eluent), and (3) two-column separation methods. The Mo contents of the USGS reference materials of basalt BIR-1a and diabase W-2a, regardless of the method used, are consistent with those reported values (Table 5). DTS-2b exhibits identical Mo contents to DTS-1 (Table 5), although these two USGS standards produced in different batches show significant differences in major and trace elements (Raczek et al., 2001). Mo contents of peridotite WPR-1 were essentially identical at 240–250 ppb, while GPt-3 results were more variable at 31–56 ppb (Table S1, Supplementary materials). $\delta^{98/95}$Mo values obtained using methods (1)–(3) for reference material BIR-1a were −0.19‰ ± 0.08‰ (2σ; n = 10), −0.21‰ ± 0.05‰ (2σ; n = 8), and −0.18‰ ± 0.06‰ (2σ; n = 9), respectively (Table 5), which are all consistent within analytical uncertainty (Fig. 5a). These values are similar to but slightly lighter than those reported by Burkhardt et al. (2014) (−0.11‰ ± 0.03‰; 2σ; n = 3) and Willbold et al. (2015) (−0.12‰ ± 0.03‰; 2σ; n = 3), possibly due to the other studies involving fewer duplicates from independent digestions. $\delta^{98/95}$Mo values of dunite DTS-2b determined by methods (1)–(3) were similar at −0.18‰ ± 0.05‰ (2σ; n = 4), −0.15‰ ± 0.05‰ (2σ; n = 5), and −0.15‰ ± 0.04‰ (2σ; n = 7), respectively (Fig. 5b), consistent with the $\delta^{98/95}$Mo values of DTS-1 obtained by Liang et al. (2017) (−0.14‰ ± 0.08‰; 2σ; n = 3). The precision of our $\delta^{98/95}$Mo results is thus comparable to that of analyses of Mo-rich reference materials, with the double- or single-column methods requiring less time and effort to produce highly reproducible and accurate results.

USGS diabase W-2a has been widely used as a geological reference material for various analyses (Burkhardt et al., 2014; Bezard et al., 2016; Zhao et al., 2016; Gaschnig et al., 2017; Li et al., 2019). The $\delta^{98/95}$Mo values obtained for W-2a here, using methods (1)–(3), were

Table 5
Mo isotopic compositions of geological reference materials from this study and the literature.

Reference material	Type	N[a,b]	Mo (ppm)	2σ	$\delta^{98/95}$Mo	2σ	Method	Origin
BIR-1a (USGS)	Basalt	10[a]	0.035	0.004	−0.19	0.08	Single-column (HCl)	This study
		8[a]	0.034	0.004	−0.21	0.05	Single-column (HNO_3)	This study
		9[a]	0.033	0.01	−0.18	0.06	Two-column	This study
		3[b]	0.032	0.005	−0.12	0.03	Single-column	Willibold et al. 2015
		4[b]	0.032		−0.11	0.03	Three-column	Burkhardt et al., 2014
DTS-2b (USGS)	Dunite	4[a]	0.029	0.007	−0.18	0.05	Single-column (HCl)	This study
		5[a]	0.026	0.001	−0.15	0.05	Single-column (HNO_3)	This study
		7[a]	0.028	0.01	−0.15	0.04	Two-column	This study
DTS-1 (USGS)	Dunite	3[a]	0.03	0.008	−0.14	0.08	Two-column	Liang et al., 2017
W-2a (USGS)	Diabase	10[a]	0.42	0.01	−0.07	0.05	Single-column (HCl)	This study
		16[a]	0.41	0.006	−0.07	0.05	Single-column (HNO_3)	This study
		3[a]	0.42	0.02	−0.06	0.01	Two-column	This study
		4[a]	0.46	0.04	−0.1	0.08	Single-column (HCl)	Zhao et al., 2016
		5[a]	0.43	0.04	−0.03	0.03	Single-column (HCl)	Li et al., 2019
		6[a]	0.40	0.009	−0.04	0.03	Three-column	Bezard et al., 2016
		2[b]	0.39		−0.05	0.06	Three-column	Burkhardt et al., 2014
		1	0.45		−0.04	0.08	Single-column	Gaschnig et al., 2017
WPR-1 (CCRMP)	Peridotite	7[a]	0.24	0.009	0.12	0.07	Single-column (HCl)	This study
		8[a]	0.24	0.01	0.12	0.07	Single-column (HNO_3)	This study
		8[a]	0.24	0.01	0.11	0.07	Two-column	This study
GPt-3 (GBW07290) (NRCG)	Dunite	4[a]	0.040	0.02	−0.14	0.16	Single-column (HCl)	This study
		7[a]	0.034	0.007	−0.07	0.24	Single-column (HNO_3)	This study
		10[a]	0.040	0.01	−0.09	0.12	Two-column	This study

[a] Number of independent digests of each geological reference material.
[b] Number of analyses.

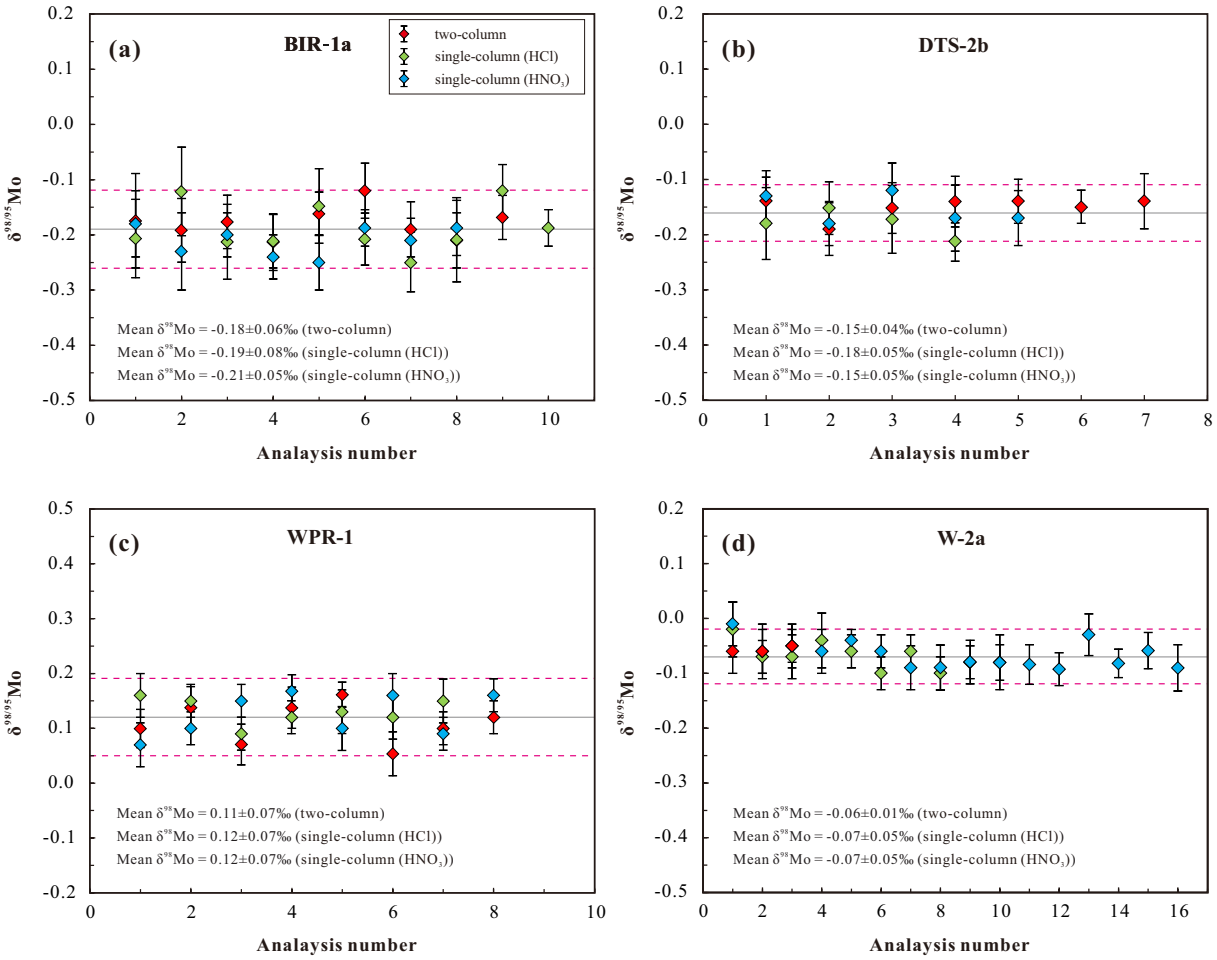

Fig. 5. Long-term stabilities of $\delta^{98/95}$Mo data for silicate rock standards of various rock types and Mo contents (see Table S1, Supplementary materials): BIR-1a (a), DTS-2b (b), WPR-1 (c) and W-2a (d). Grey solid lines indicate mean $\delta^{98/95}$Mo values; pink dashed lines indicate ± 2σ from the mean. (For interpretation of the references to colour in this figure legend, the reader is referred to the web version of this article.)

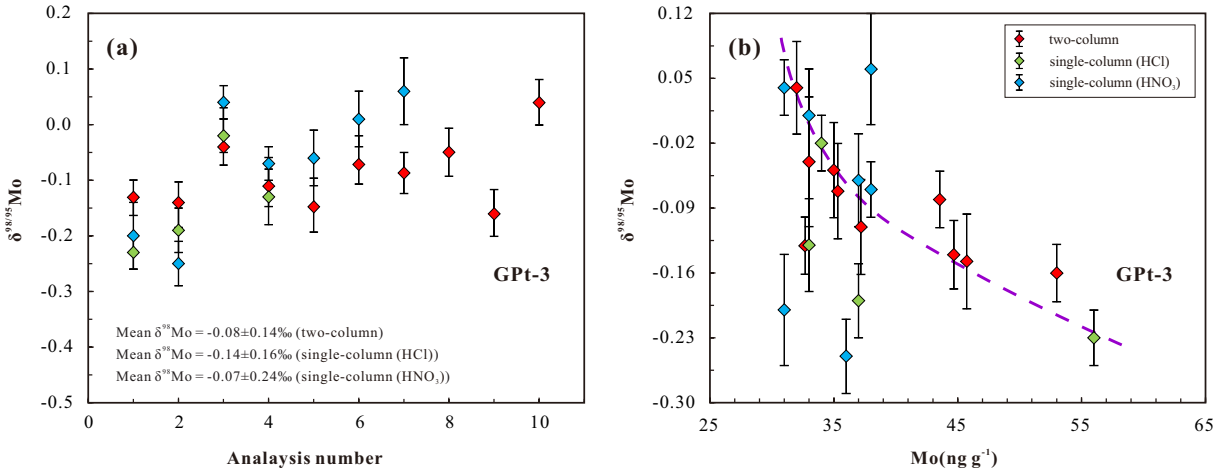

Fig. 6. (a) Variations in $\delta^{98/95}$Mo values in reference material GPt-3; and (b) $\delta^{98/95}$Mo values versus Mo content.

identical at −0.07‰ ± 0.05‰ (2σ; n = 10), −0.07‰ ± 0.05‰ (2σ; n = 16), and −0.06‰ ± 0.01‰ (2σ; n = 3), respectively, (Fig. 5d) all within uncertainty of reported values (Table 5) and confirming that Mo isotopic compositions can be determined accurately using the methods described here.

Peridotite WPR-1 and dunite GPt-3 are commonly used as reference materials in analyses of platinum group elements, and this is the first report of their Mo isotopic compositions as determined by the different methods: $\delta^{98/95}Mo_{WPR\text{-}1}$ = 0.12‰ ± 0.07‰ (method 1; 2σ; n = 7), 0.12‰ ± 0.07‰ (method 2; 2σ; n = 8), and 0.11‰ ± 0.07‰ (method 3; 2σ; n = 8); $\delta^{98/95}Mo_{GPt\text{-}3}$ = −0.14‰ ± 0.16‰ (method 1; 2σ; n = 4), −0.07‰ ± 0.24‰ (method 2; 2σ; n = 4), and −0.09‰ ± 0.12‰ (method 3; 2σ; n = 10). The near-identical $\delta^{98/95}$Mo values of WPR-1 (Fig. 5c) mean it can be recommended for use as a reference material for Mo isotopic composition. However, for the $\delta^{98/95}$Mo values of GPt-3, these three methods gave poor reproducibility (Fig. 6a). The plot of GPt-3 $\delta^{98/95}$Mo values versus Mo content indicates a weak negative correlation (Fig. 6b), suggesting that the GPt-3 powder is heterogeneous in terms of content and isotopic composition, as has been reported in Re−Os isotopic analyses (Shen et al., 2019). This heterogeneity does not reflect contamination by abraded material during preparation of the rock powder, which would have significantly affected the Mo content (Willbold et al., 2015). Rather, as GPt-3 is a Mg-rich ultrabasic rock (from North Qilian) associated with chromite mineralization, the heterogeneous distribution of some Mo-bearing minerals (e.g., chromite and sulfide) may well account for variations in Mo content and isotopic composition. In addition, inadequately digestion of the refractory spinel phases using normal-pressure beaker digestion method may also result in the heterogeneity of GPt-3, although it is uncertain if the spinel hosts significant Mo.

In conclusion, the four rock reference standards (BIR-1, DTS-2b, W-2a, and WPR-1) with variable Mo contents yielded $\delta^{98/95}$Mo values with high precision and good reproducibility when using either double- or single-column separation techniques, indicating that our methods are capable of processing igneous samples, especially low-Mo rocks. The single-column method shows slightly lower blanks and is less time consuming. However, the double-column chemistry can rinse off some major matrix elements (e.g., Fe, Ni, Cr, Co, Mn, Cu and Sr) twice, which can really guarantee highly accurate measurements. Thus, we suggest the double column procedure for low-Mo samples with high contents of Fe, Ni, Cr, Co, Mn, Cu and Sr.

4. Mo isotopic composition of leucogranites from Tibet

Leucogranites, occurring widely in collisional orogen (e.g., Tartèse and Boulvais, 2010; Philipp et al., 2013; Paul et al., 2014; Wu et al., 2020), are one of the most important components of Earth's continental crust. Investigating their Mo content and isotopic composition may improve our understanding of the compositional evolution of continental crust.

Leucogranite samples from the Himalaya orogen and southern Lhasa terrane have low Mo contents of 10–74 ppb (Table 6). Tonalite–trondhjemite–granodiorite rocks (TTGs) from the Superior Province and Zimbabwe craton are also significantly depleted in Mo (< 100 ppb; Luais and Hawkesworth, 1994; Whalen et al., 2002, 2003). Greaney et al. (2018) ascribed this depletion to fractionating titaniferous phases such as rutile and Fe−Ti oxides, and/or Mo loss from source detrital sediments through oxidative weathering. The Himalaya leucogranites exhibit Sr−Nd isotopic compositions that differ from those of the Zhengga leucogranites (Fig. 7a), indicating different sources. The former have been considered pure crustal melts derived from partial melting of metasediments (Hopkinson et al., 2017), while the latter

Table 6
Mo elemental and isotopic composition with selected elemental and Sr−Nd isotope data of the leucogranites from the Himalaya and southern Lhasa.

Sample	Lithology	$\delta^{98/95}$Mo	2se	Mo (ppm)	Method
Saga, Himalaya					
LBKR-2	TMG	−0.07	0.04	0.053	two-column
LBKR-3	TMG	0.03	0.08	0.015	two-column
LB03	GBG	−1.43	(0.05, n = 3)[a]	0.045	two-column
Tsona, Himalaya					
SN35-2	TMG	0.36	0.07	0.012	two-column
SN35-2 replicate		0.31	0.06	0.010	single-column (HNO_3)
SN36-4	TMG	−0.07	0.06	0.017	two-column
SN36-4 replicate		−0.06	0..07	0.021	single-column (HNO_3)
SN58-1	TMG	−0.20	0.07	0.019	two-column
SN58-4	TMG	0.04	0.06	0.019	two-column
SN58-4 replicate		0.04	0.07	0.020	single-column (HNO_3)
SN36-1	GBG	−0.15	0.08	0.020	two-column
SN34-5	GBG	0.17	0.08	0.013	two-column
Zhengga, Southern Lhasa					
ML06-1	GBG	−0.54	0.05	0.047	two-column
SR01-2	GBG	−0.67	0.05	0.070	single-column (HCl)
ML08-2	GBG	−0.41	0.07	0.029	two-column
SR05-3	GBG	−0.64	0.05	0.063	two-column
SR05-3 replicate		−0.68	0.03	0.074	single-column (HCl)

Replicate: repeat digests of the same sample powder.
[a] Twice the standard deviation of the $\delta^{98/95}$Mo value of LB03 obtained by independent digestion 3 times.

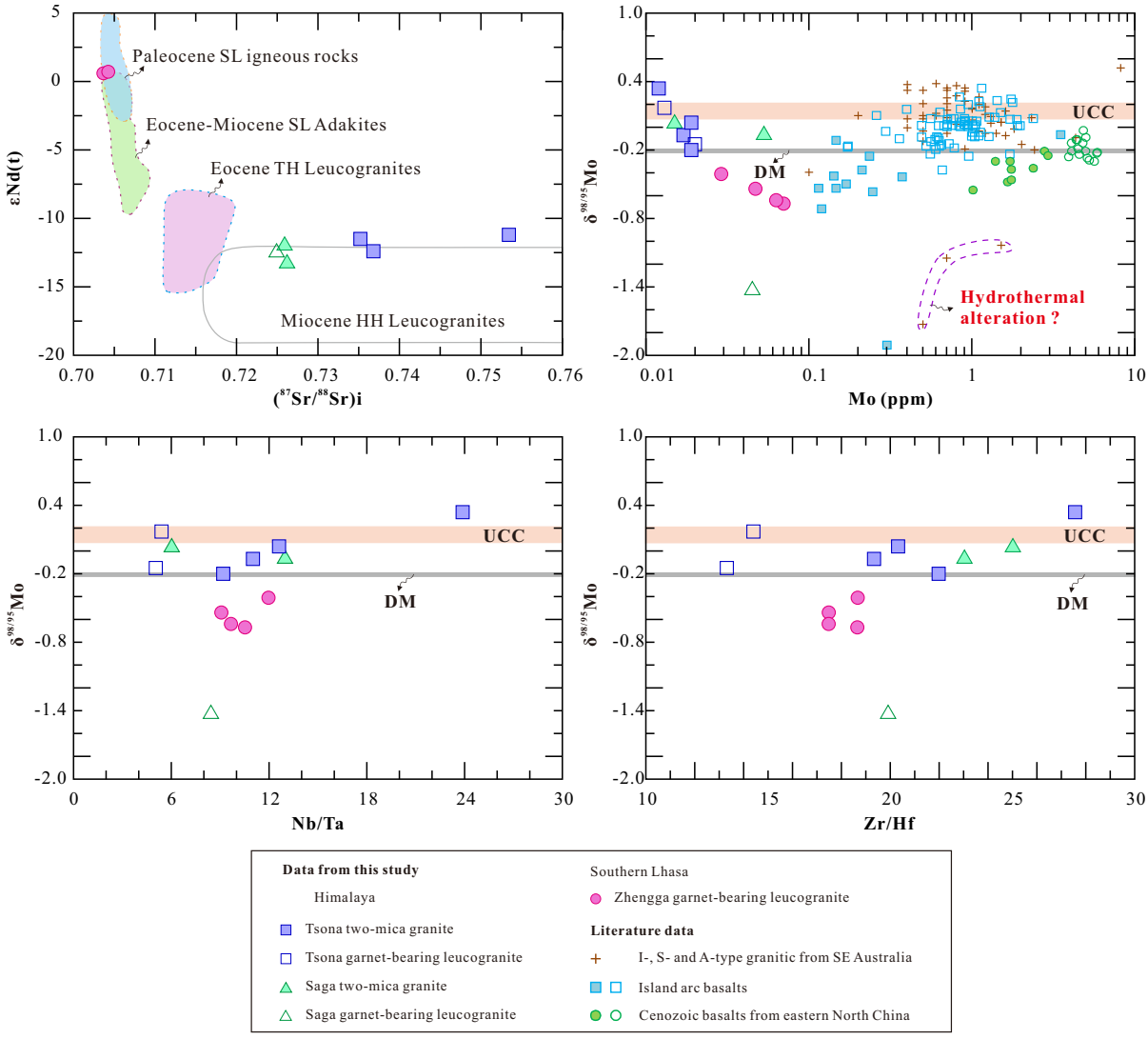

Fig. 7. (a) $(^{87}Sr/^{86}Sr)_i$ vs. εNd(t); and (b–d) $\delta^{98/95}$Mo vs Mo content, (Nb/Ta), and (Zr/Hf) for the leucogranites of this study. Data for Zhengga GBGs, Miocene High Himalaya (HH) leucogranites, Eocene Tethys Himalaya (TH) granites, and Eocene–Miocene South Lhasa (SL) adakites are from Ma et al. (2018) and references therein. Sr-Nd isotopic data and Nb/Ta, Zr/Hf ratios of the Himalayan leucograites in this study are from the unpublished data. Data for island arc basalts and Cenozoic basalts from eastern North China are from Voegelin et al. (2014), Freymuth et al. (2015, 2016), König et al. (2016), and Li et al. (2019). Solid symbols indicate involvement of more sediment melt in the mantle source. The $\delta^{98/95}$Mo values for the I-, S- and A-type granites from SE Australia, depleted mantle (DM) and upper continental crust (UCC) are from Bezard et al. (2016) and Yang et al. (2017).

were generated by fractionation of biotite granite magmas that were derived predominantly from juvenile lower crust (Ma et al., 2018).

MC–ICP–MS Mo isotopic analyses of leucogranite samples from the Himalaya orogen and southern Lhasa terrane yielded $\delta^{98/95}$Mo values of −1.43‰ to 0.34‰ and −0.41‰ to −0.67‰, respectively. The Himalaya leucogranites have Mo isotopic compositions similar to those of Australian I-, S-, and A-type granites (Yang et al., 2017), deviating slightly from upper continental crust (UCC) compositions (Fig. 7b). In comparison, the Zhengga leucogranites have $\delta^{98/95}$Mo values lower than those estimated for depleted mantle, but similar to those of arc basalts with sedimentary components (Fig. 7b). The effects of fractional crystallization on Mo isotopic fractionation remain debatable. Previous studies have suggested that Mo isotopes can be fractionated during differentiation of water-rich calc-alkaline arc magmas (Voegelin et al., 2014; Wille et al., 2018), while a lack of isotopic fractionation was observed in dry Hekla volcanic rocks and less-differentiated MORB (Yang et al., 2015; Bezard et al., 2016). The $\delta^{98/95}$Mo values of the GBGs and TMGs show no obvious variation trend with indices of granitic differentiation (e.g., Zr/Hf and Nb/Ta ratios; Fig. 7c, d), suggesting either that fractional crystallization cannot account fully for their Mo isotopic compositions, or that their compositional diversity cannot be explained by crystallization differentiation. One GBG sample from the Saga area has an anomalously light Mo isotopic composition, and similar values occur in granitic rocks from Scotland (Fig. 7b) where they have been ascribed to hydrothermal alteration (Yang et al., 2017). However, this is not clear for the GBG sample as no obvious alteration was observed. The contrasting Mo isotopic compositions of the Himalaya and Zhengga leucogranites could result from their having different sources, as indicated by their Sr−Nd isotopic compositions (Fig. 7a), although further data are required to assess the effects of assimilation–fractionation–crystallization (AFC) processes. Our results expand the small available database for high-precision $\delta^{98/95}$Mo analyses of low-Mo granites, and highlight the need for further analyses to provide a better understanding of the Mo isotopic composition of continental crust.

5. Conclusions

Two low-blank, high-recovery, and high-efficiency analytical methods described here provided precise and accurate Mo isotopic compositions for low-Mo (10–500 ppb) igneous rocks. The double-column isolation technique is less time-consuming (8 h) than previously published methods. The improved procedure with single BPHA column may be the most efficient Mo isolation method for geological samples to date. The data quality of our methods are comparable to the other procedures (Burkhardt et al., 2014; Willbold et al., 2015; Bezard et al., 2016; Gaschnig et al., 2017) either for high-Mo or low-Mo samples. Based on repeated analysis of the geological reference materials, the long-term external reproducibility of Mo isotopic compositions can be better than ± 0.05‰ (2σ). We first measured the $\delta^{98/95}$Mo values of the rock standards of peridotite WPR-1 and dunite DTS-2b which show good reproducibility. The two methods for Mo purification achieve measurement of the $\delta^{98/95}$Mo values of the leucogranites with ultra-low Mo contents (10–74 ppb) from the Himalaya orogen and southern Lhasa terrane. Our study of their Mo isotopic compositions highlights a need for further extension of the high-precision Mo isotopic database for leucogranites, to improve understanding of the Mo isotopic composition of continental crust.

Supplementary data to this article can be found online at https://doi.org/10.1016/j.chemgeo.2020.119648.

Declaration of competing interest

The authors declare that they have no known competing financial interests or personal relationships that could have appeared to influence the work reported in this paper.

Acknowledgements

We appreciate the assistance of Xiang-Lin Tu for elemental signal measurements, and Dr. Zhi-Bing Wang for his helpful suggestions on the work prior to chemical separation. We also grateful to editor Balz Kamber and the two anonymous reviewers, whose insightful and constructive reviews/editorial advice greatly improve this manuscript. This work was supported by the National Key Research and Development Program of China (2016YFC0600407), the National Natural Science Foundation of China (41630208 and 91855215), the Key Program of the Chinese Academy of Sciences (QYZDJ-SSW-DQC026), the Key Program of Guangzhou City (No. 201604910124), the National Science Foundation of China (41673008) and the Key Technical Talents of Chinese Academy of Sciences (CAS) for Li Jie, and the Guangzhou Institute of Geochemistry, Chinese Academy of Science (GIGCAS 135 project 135TP201601). This is contribution No. IS-2860 from GIGCAS.

References

Anbar, A.D., 2004. Molybdenum stable isotopes: observations, interpretations and directions. Rev. Mineral. Geochem. 55, 429–454.
Anbar, A.D., Knab, K.A., Barling, J., 2001. Precise determination of mass-dependent variations in the isotopic composition of molybdenum using MC–ICP–MS. Anal. Chem. 73, 1425–1431.
Barling, J., Arnold, G.L., Anbar, A.D., 2001. Natural mass-dependent variations in the isotopic composition of molybdenum. Earth Planet. Sci. Lett. 193, 447–457.
Bezard, R., Fischer-Gödde, M., Hamelin, C., Brennecka, G.A., Kleine, T., 2016. The effects of magmatic processes and crustal recycling on the molybdenum stable isotopic composition of Mid-Ocean Ridge Basalts. Earth Planeta. Sci. Lett. 453, 171–181.
Burkhardt, C., Hin, R.C., Kleine, T., Bourdon, B., 2014. Evidence for Mo isotope fractionation in the solar nebula and during planetary differentiation. Earth Planet. Sci. Lett. 391, 201–211.
Caletka, R., Krivan, V., 1989. Extraction of molybdenum and tungsten with various reagents. Fresenius' Z. Anal. Chem. 332, 866–873.
Casalini, M., Avanzinelli, R., Tommasini, S., Elliott, T., Conticelli, S., 2019. Ce/Mo and molybdenum isotope systematics in subduction-related orogenic potassic magmas of Central-Southern Italy. Geochem. Geophy. Geosy. 20, 2753–2768.
Chen, S., Hin, R.C., John, T., Brooker, R., Bryan, B., Niu, Y.L., Elliott, T., 2019. Molybdenum systematics of subducted crust record reactive fluid flow from underlying slab serpentine dehydration. Nat. Commun. 10, 4773.
Dauphas, N., Reisberg, L., Marty, B., 2001. Solvent extraction, ion chromatography, and mass spectrometry of molybdenum isotopes. Anal. Chem. 73, 2613–2616.
Dickson, A.J., 2017. A molybdenum-isotope perspective on Phanerozoic deoxygenation events. Nat. Geosci. 10, 721–726.
Feng, L.P., Zhou, L., Hu, W.F., Zhang, W., Li, B.C., Liu, Y.S., Hu, Z.C., Yang, L., 2019. A simple single-stage extraction method for Mo separation from geological samples for isotopic analysis by MC–ICP–MS. J. Anal. At. Spectrom. 35, 145–154.
Freymuth, H., Vils, F., Willbold, M., Taylor, R.N., Elliot, T., 2015. Molybdenum mobility and isotopic fractionation during subduction at the Mariana arc. Earth Planet. Sci. Lett. 432, 176–186.
Freymuth, H., Elliott, T., van Soest, M., Skora, S., 2016. Tracing subducted black shales in the Lesser Antilles arc using molybdenum isotope ratios. Geology 44, 987–990.
Gaschnig, R.M., Reinhard, C.T., Planavsky, N.J., Wang, X., Asael, D., Chauvel, C., 2017. The molybdenum isotope system as a tracer of slab input in subduction zones: an example from Martinique, Lesser Antilles Arc. Geochem. Geophy. Geosy. 18, 4674–4689.
Goguel, R., 1992. Group separation by solvent extraction from silicate rock matrix of Nb, Mo, Ta and W at low levels for ICP-MS. Fresenius' Journal of Anal. Chem. 344, 326–333.
Gordon, G.W., Lyons, T.W., Arnold, G.L., Roe, J., Sageman, B.B., Anbar, A.D., 2009. When do black shales tell molybdenum isotope tales? Geology 37, 535–538.
Greaney, A.T., Rudnick, R.L., Gaschnig, R.M., Whalen, J.B., John, B.L., Clemens, D., 2018. Geochemistry of molybdenum in the continental crust. Geochim. Cosmochim. Acta 238, 36–54.
Greber, N.D., Puchtel, I.S., Nägler, T.F., Mezger, K., 2015. Komatiites constrain molybdenum isotope composition of the Earth's mantle. Earth Planet. Sci. Lett. 421, 129–138.
Helz, G.R., Miller, C.V., Charnock, J.M., Mosselmans, J.F.W., Pattrick, R.A.D., Garner, C.D., Vaughan, D.J., 1996. Mechanism of molybdenum removal from the sea and its concentration in black shales: EXAFS evidence. Geochim. Cosmochim. Acta 60, 3631–3642.
Hopkinson, T.N., Harris, N.B.W., Warren, C.J., Spencer, C.J., Roberts, N.M.W., Horstwood, M.S.A., Parrish, R.R., EIMF, 2017. The identification and significance of pure sediment-derived granites. Earth Planet. Sci. Lett. 467, 57–63.
Jenner, F.E., O'Neill, H.St.C, 2012. Major and trace analysis of basaltic glasses by laser-ablation ICP-MS. Geochem. Geophys. Geosyst. 13, Q03003.
König, S., Wille, M., Voegelin, A., Schoenberg, Ronny, 2016. Molybdenum isotope systematics in subduction zones. Earth Planet. Sci. Lett. 447, 95–102.
Li, J., Zhong, L.F., Tu, X.L., Liang, X.R., Xu, J.F., 2010. Determination of rhenium content in molybdenite by ICPMS after separation of the major matrix by solvent extraction with N-benzoyl-N-phenylhydroxalamine. Talanta 81, 954–958.
Li, J., Liang, X.R., Zhong, L.F., Wang, X.C., Ren, Z.Y., Sun, S.L., Zhang, Z.F., Xu, J.F., 2014. Measurement of the isotopic composition of molybdenum in geological samples by MC–ICP–MS using a novel chromatographic extraction technique. Geostand. Geoanal. Res. 38, 345–354.
Li, H.Y., Li, J., Ryan, J.G., Li, X., Zhao, R.P., Ma, L., Xu, Y.G., 2019. Molybdenum and boron isotope evidence for fluid-fluxed melting of intraplate upper mantle beneath the eastern North China Craton. Earth Planet. Sci. Lett. 520, 105–114.
Liang, Y.H., Halliday, A.N., Siebert, C., Fitton, J.G., Burton, K.W., Wang, K.L., Harvey, J., 2017. Molybdenum isotope fractionation in the mantle. Geochim. Cosmochim. Acta 199, 91–111.
Liu, J., Wen, H.J., Zhang, Y.X., Fan, H.F., Zhu, C.W., 2016. Precise Mo isotope ratio measurements of low-Mo (ng g^{-1}) geological samples using MC–ICP–MS. J. Anal. At. Spectrom. 31, 1287–1297.
Luais, B., Hawkesworth, C.J., 1994. The generation of continental crust: an integrated study of crust-forming processes in the Archaean of Zimbabwe. J. Petrol. 35, 43–93.
Ma, L., Wang, Q., Kerr, A.C., Yang, J.H., Xia, X.P., Ou, Q., Yang, Z.Y., Sun, P., 2018. Paleocene (ca. 62 Ma) leucogranites in southern Lhasa, Tibet: products of syn-collisional crustal anatexis during slab roll-back? J. Petrol. 58, 2089–2114.
Malinovsky, D., Rodushkin, I., Baxter, D.C., Ingri, J., Ohlander, B., 2005. Molybdenum isotope ratio measurements on geological samples by MC–ICP–MS. Int. J. Mass Spectrom. 245, 94–107.
McManus, J., Nägler, T.F., Siebert, C., Wheat, C.G., Hammond, D.E., 2002. Oceanic molybdenum isotope fractionation: diagenesis and hydrothermal ridge-flank alteration. Geochem. Geophys. Geosyst. 3, 1–9.
Nakagawa, Y., Firdaus, M.L., Norisuye, K., Sohrin, Y., Irisawa, K., Hirata, T., 2008. Precise isotopic analysis of Mo in seawater using multiple collector-inductively coupled mass spectrometry coupled with a chelating resin column preconcentration method. Anal. Chem. 80, 9213–9219.
Palme, H., O'Neill, H.St.C, 2004. Cosmochemical estimates of mantle composition. In: Holland, H.D., Turrekian, K.K. (Eds.), Treatise on Geochemistry. 2. pp. 1–38.
Paul, A., Jung, S., Romer, R.L., Stracke, A., Hauff, F., 2014. Petrogenesis of synorogenic high-temperature leucogranites (Damara orogen, Namibia): constraints from U–Pb monazite ages and Nd, Sr and Pb isotopes. Gondwana Res. 25, 1614–1626.
Pearce, C.R., Cohen, A.S., Coe, A.L., Burton, K.W., 2008. Molybdenum isotope evidence for global ocean anoxia coupled with perturbations to the carbon cycle during the Early Jurassic. Geology 36, 231–234.
Pearce, C.R., Cohen, A.S., Parkinson, I.J., 2009. Quantitative separation of molybdenum and rhenium from geological materials for isotopic analysis by MC–ICP–MS. Geostand. Geoanal. Res. 33, 219–229.
Philipp, R.P., Massonne, H.J., Campos, R.S.D., 2013. Peraluminous leucogranites of the Cordilheira Suite: a record of Neoproterozoic collision and the generation of the Pelotas Batholith, Dom Feliciano Belt, Southern Brazil. J. S. Am. Earth Sci. 43, 8–24.
Pietruszka, A.J., Reznik, A.D., 2008. Identification of a matrix effect in the MC–ICP–MS due to sample purification using ion exchange resin: an isotopic case study of

molybdenum. Int. J. Mass Spectrom. 270, 23–30.
Pietruszka, A.J., Walker, R.J., Candela, P.A., 2006. Determination of mass-dependent molybdenum isotopic variations by MC–ICP–MS: an evaluation of matrix effects. Chem. Geol. 225, 121–136.
Planavsky, N.J., Asael, D., Hofmann, A., Reinhard, C.T., Lalonde, S.V., Knudsen, A., Wang, X., Ossa, F., Pecoits, E., Smith, A.J.B., Beukes, N.J., Bekker, A., Johnson, T.M., Konhauser, K.O., Lyons, T.W., Rouxel, O.J., 2014. Evidence for oxygenic photosynthesis half a billion years before the Great Oxidation Event. Nat. Geosci. 7, 283–286.
Qi, L., Masuda, A., 1994. The isotopic composition and atomic-weight of molybdenum. Int. J. Mass Spectrom. 130, 65–72.
Raczek, I., Stoll, B., Hofmann, A.W., Jochum, K.P., 2001. High-precision trace element data for the USGS reference materials BCR-1, BCR-2, BHVO-1, BHVO-2, AGV-1, AGV-2, DTS-1, DTS-2, GSP-1 and GSP-2 by ID-TIMS and MIC-SSMS. Geostand. Geoanal. Res. 25, 77–86.
Rudge, J.F., Reynolds, B.C., Bourdon, B., 2009. The double spike toolbox. Chem. Geol. 265, 420–431.
Scott, C., Lyons, T.W., 2012. Contrasting molybdenum cycling and isotopic properties in euxinic versus non-euxinic sediments and sedimentary rocks: refining the paleoproxies. Chem. Geol. 324–325, 19–27.
Shen, X.Y., Li, J., Xu, J.F., Sun, S.L., 2019. Precise determination of the platinum-group elements and Re-Os isotopic compositions in national reference samples GPt-3 and GPt-4. Geochimica 48, 395–402 (Chinese with English abstract).
Shinotsuka, K., Suzuki, K., 2007. Simultaneous determination of platinum-group elements and rhenium in rock samples using isotope dilution inductively coupled plasma-mass spectrometry after cation exchange separation followed by solvent extraction. Anal. Chim. Acta 603, 129–139.
Siebert, C., Nagler, T.F., Kramers, J.D., 2001. Determination of molybdenum isotope fractionation by double-spike multicollector inductively coupled mass spectrometry. Geochem. Geophy. Geosy. 2.
Siebert, C., Nägler, T.F., von Blankenburg, F., Kramers, J.D., 2003. Molybdenum isotope records as a potential new proxy for paleoceanography. Earth Planet. Sci. Lett. 211, 159–171.
Tartèse, R., Boulvais, P., 2010. Differentiation of peraluminous leucogranites 'en route' to the surface. Lithos 114, 353–368.
Tossell, J.A., 2005. Calculating the partitioning of the isotopes of Mo between oxidic and sulfidic species in aqueous solution. Geochim. Cosmochim. Acta 69, 2981–2993.
Voegelin, A.R., Nägler, T.F., Samankassou, E., Villa, I.M., 2009. Molybdenum isotopic composition of modern and Carboniferous carbonates. Chem. Geol. 265, 488–498.
Voegelin, A.R., Nägler, T.F., Pettke, T., Neubert, N., Steinmann, M., Pourret, O., Villa, I.M., 2012. The impact of igneous bedrock weathering on the Mo isotopic composition of stream waters: natural samples and laboratory experiments. Geochim. Cosmochim. Acta 86, 150–165.
Voegelin, A.R., Pettke, T., Greber, N.D., von Niederhäusern, B., Nägler, T.F., 2014. Magma differentiation fractionates Mo isotope ratios: evidence from the Kos Plateau Tuff (Aegean Arc). Lithos 190–191, 440–448.
Wasylenki, L.E., Rolfe, B.A., Weeks, C.L., Spiro, T.G., Anbar, A.D., 2008. Experimental investigation of the effects of temperature and ionic strength on Mo isotope fractionation during adsorption to manganese oxides. Geochim. Cosmochim. Acta 72, 5997–6005.
Wen, H.J., Fan, H.F., Zhang, Y.X., Cloquet, C., Carignan, J., 2015. Reconstruction of early Cambrian ocean chemistry from Mo isotopes. Geochim. Cosmochim. Acta 164, 1–16.
Whalen, J.B., Percival, J.A., McNicoll, V.J., Longstaffe, F.J., 2002. A mainly crustal origin for tonalitic granitoid rocks, Superior Province, Canada: implications for Late Archean tectonomagmatic processes. J. Petrol. 43, 1551–1570.
Whalen, J.B., Percival, J.A., McNicoll, V.J., Longstaffe, F.J., 2003. Intra-oceanic production of continental crust in a Thdepleted ca. 3.0 Ga arc complex, western Superior Province, Canada. Contrib. Mineral. Petrol. 146, 78–99.
Willbold, M., Hibbert, K., Lai, Y.J., Freymuth, H., Hin, R.C., Coath, C., Vils, F., Elliott, T., 2015. High-precision mass-dependent molybdenum isotope variations in magmatic rocks determined by double-spike MC–ICP–MS. Geostand. Geoanal. Res. 40, 389–403.
Wille, M., Nebel, O., Pettke, T., Vroon, P.Z., KöNig, S., Schoenberg, R., 2018. Molybdenum isotope variations in calc-alkaline lavas from the Banda arc, Indonesia: assessing the effect of crystal fractionation in creating isotopically heavy continental crust. Chem. Geol. 485, 1–13.
Wu, F.Y., Liu, X.C., Liu, Z.C., Wang, R.C., Xie, L., Wang, J.M., Ji, W.Q., Yang, L., Liu, C., Khanal, G.P., He, S.X., 2020. Highly fractionated Himalayan leucogranites and associated rare-metal mineralization. Lithos 352–353.
Yang, X.J., Pin, C., 2002. Determination of niobium, tantalum, zirconium and hafnium in geological materials by extraction chromatography and inductively coupled plasma-mass spectrometry. Anal. Chim. Acta 458, 375–386.
Yang, J., Siebert, C., Barling, J., Savage, P., Liang, Y.H., Halliday, A.N., 2015. Absence of molybdenum isotope fractionation during magmatic differentiation at Hekla volcano, Iceland. Geochim. Cosmochim. Acta 162, 126–136.
Yang, J., Barling, J., Siebert, C., Fietzke, J., Stephens, E., Halliday, A.N., 2017. The molybdenum isotopic compositions of I-, S- and A-type granitic suites. Geochim. Cosmochim. Acta 205, 168–186.
Zhang, Y.X., Wen, H.J., Fan, H.F., 2009. Chemical pretreatment methods for measurement of Mo isotope ratio on geological samples. (Chinese Journal of Analytical Chemistry) Anal. Chem. 37, 216–220.
Zhang, L., Ren, Z.Y., Xia, X.P., Li, J., Zhang, Z.F., 2015. Isotope maker: a Matlab program for isotopic data reduction. Int. J. Mass Spectrom. 392, 118–124.
Zhang, L., Li, J., Xu, Y.G., Ren, Z.Y., 2018. The influence of the double spike proportion effect on stable isotope (Zn, Mo, Cd, and Sn) measurements by multicollector-inductively coupled plasma-mass spectrometry (MC–ICP–MS). J. Anal. Atom. Spectrom. 33, 555–562.
Zhang, Y.Y., Yuan, C., Sun, M., Li, J., Long, X.P., Jiang, Y.D., Huang, Z.Y., 2019. Molybdenum and boron isotopic evidence for carbon-recycling via carbonate dissolution in subduction zones. Geochim. Cosmochim. Acta (In press).
Zhao, P.P., Li, J., Zhang, L., Wang, Z.B., Kong, D.X., Ma, J.L., Wei, G.J., Xu, J.F., 2016. Molybdenum mass fractions and isotopic compositions of international geological reference materials. Geostand. Geoanal. Res. 40, 217–226.